Multi-temporal mapping of burned forest over Canada

using satellite-based change metrics

R.H. Fraser, R. Fernandes, and R. Latifovic

Natural Resources Canada, Canada Centre for Remote Sensing

588 Booth St., Ottawa, ON, Canada, K1A 0Y7

robert.fraser@ccrs.nrcan.gc.ca

Abstract

A procedure for continental-scale mapping of burned boreal forest at 10-day intervals was developed for application to coarse resolution satellite imagery. The basis of the technique is a multiple logistic regression model parameterized using 1998 SPOT-4 VEGETATION clear-sky composites and training sites selected across Canada. Predictor features consisted of multi-temporal change metrics based on reflectance and two vegetation indices, which were normalized to the trajectory of background vegetation to account for phenological variation. Spatial-contextual tests applied to the logistic model output were developed to remove noise and increase the sensitivity of detection. The procedure was applied over Canada for the 1998-2000 fire seasons and validated using fire surveys and burned area statistics from forest fire management agencies. The area of falsely mapped burns was found to be small (3.5% commission error over Canada), and most burns larger than 10 km^2 were accurately detected and mapped ($R^2 = 0.90$, $P<0.005$, n = 91 for burns in two provinces). Canada-wide satellite burned area was similar, but consistently smaller by comparison to statistics compiled by the Canadian Interagency Forest Fire Centre (by 17% in 1998, 16% in 1999, and 3% in 2000).

INTRODUCTION

Biomass burning causes a wide range of global environmental impacts. The destruction of vegetation by fire modifies the land/atmosphere carbon balance, changes the Earth's albedo, and releases aerosols that affect climate and radiation budget (Crutzen and Andreae, 1990). Fires also have direct effects on human populations due to episodic smoke pollution and the loss of valuable forest resources (Siegert and Hoffmann, 2000; FAO, 2001). To help quantify the magnitude of these impacts, the most comprehensive, recent estimates of worldwide biomass burning were compiled by the Food and Agriculture Organisation and reported in the Global Forest Fire Assessment 1990-2000 (FAO, 2001). This report includes forest burned area statistics, but which are spatially lumped and available for only a minority of countries covered in the report.

To improve the level of available information on the distribution of biomass burning, the Joint Research Centre (JRC) of the European Commission is leading an international initiative aimed at producing spatially explicit, global burned area maps from satellite remote sensing. The Global Burned Area 2000 (GBA 2000) project involves a collaboration of seven research institutes that have developed regional algorithms to map monthly burned areas in 2000 using SPOT VEGETATION (VGT) imagery. It is anticipated that the 1 km resolution burned area products will help serve the needs of the scientific community for modelling fire emissions, terrestrial carbon budget, and land cover. This paper describes the development and validation of a GBA 2000 algorithm that was designed to map burned boreal forest in Canada.

In Canada, an average 3.4 million ha of forest burned annually during the 10-year period 1989-1998 [Canadian Interagency Forest Fire Centre (CIFFC); www.ciffc.ca]. The vast majority of this burning is attributable to lightning fires that lead to near-complete destruction of trees over large tracts of coniferous forests (Stocks, 2001). Coarse resolution imagery from NOAA's Advanced Very High Resolution Radiometer (AVHRR) has been employed in several studies to map burned area at annual intervals in the boreal zone. Cahoon et al. (1994) applied unsupervised classification to three composited AVHRR channels, supplemented with daily fire imagery, to map widespread burning in Asian forest in 1987. Kasischke and French (1995) used differencing and thresholding of pre- and post-burn AVHRR Normalized Difference Vegetation Index (NDVI) composites to map burns in Alaska. Fraser et al. (2000) developed an algorithm

that builds on this approach by using active fire locations from NOAA/AVHRR as training samples to derive change thresholds and reduce the occurrence of false burns.

The mapping technique presented here exploits imagery from the more recent SPOT VGT sensor. It was also designed to map burned areas at 10-day intervals, rather than annual intervals addressed in the previous boreal mapping work. A 10-day burned area product is suitable for meeting the GBA 2000 requirement to produce monthly burned area maps and statistics. It could allow burning events to be related to prevailing fire weather conditions, which are important in determining levels of fuel consumption and fire emissions.

SATELLITE DATA

Burned area mapping conducted under the GBA 2000 initiative uses global, daily (S1) input data from the SPOT VGT sensor. VGT provides reflectance measurements at 1 km resolution in four spectral bands (centred on 0.45 µm blue, 0.66 µm red, 0.83 µm NIR, and 1.65 µm SWIR), the last two of which in combination are highly effective for discriminating burned vegetation (Pereira, 1999). Ten-day (S10) composite imagery from the VGT sensor was used in this study to develop and test an algorithm designed for mapping burns at 10-day intervals. The Canada-wide composites cover consecutive 10-day periods from April 21 – October 10, 1998-2000, and were nominally corrected by SPOT for atmospheric effects using the Simplified Method of Atmospheric Correction SMAC (Rahman and Dedieu, 1994). The imagery was reprojected in-house to a Lambert Conformal Conic projection then normalized to a common viewing geometry to account for bi-directional reflectance distribution function effects (Latifovic et al., 2002). For final GBA 2000 processing at JRC, 10-day composites will be created by compositing S1 products based on a maximum NDVI criterion.

MODEL DEVELOPMENT

The major steps for developing the burned area mapping procedure are described below and consisted of (1) selecting training data, (2) computing satellite change metrics, (3) parameterizing a per-pixel logistic regression model, (4) deriving a threshold to convert the

logistic probability output to a binary burn product, and (5) developing contextual tests to refine the binary product.

Training data

The procedure was developed and trained using VGT data from 1998, a year in which 4.7 million ha of forest burned in Canada, or 38% more than the 10-year average. Training samples for algorithm development were selected across Canada to represent forest burned during that year (163 polygons comprising 2,466 pixels) and various forest cover types not subjected to burning (222 polygons comprising 2,637 pixels). Burned forest sites were manually identified with the aid of active fire locations derived from a boreal fire detection algorithm applied to daily 1998 AVHRR fire locations (Li et al., 2000), which were superimposed on a post-fire season VGT image from September 1998 where recent burns are readily visible. A wide range of forested pixels not subject to burning in 1998 was selected, including coniferous, deciduous, mixed coniferous-deciduous, northern transitional, and previously burned forest. This selection would ensure that the algorithm would perform well when applied to all forested pixels across Canada and to other years.

Change metrics and logistic regression modelling

Logistic regression analysis was used as the basis for the multi-temporal burned area algorithm. This statistical approach is well suited for classifying the state of a dichotomous environmental variable based on multiple explanatory variables derived from satellite imagery or other spatial data (Pereira and Itami, 1991; Luther et al., 1997; Mitchener and Houhoulis, 1997; Narumalani et al., 1997). In a fire application, Koutsias and Karteris (1998) used a logistic model for classifying burned vegetation in Greece based on reflectance measured from a pair of pre- and post-burn Landsat TM scenes, as well as a single post-burn scene (2000). Logistic models have also been developed for Canada to predict the occurrence of human caused fires using weather-based indices from the Canadian Forest Fire Danger Rating System (Martell et al., 1987; Vega Garcia et al., 1995).

In this application, a multiple logistic regression model was derived to classify the training samples described above by assigning burned pixels a value of 1 and unburned pixels a

value of 0. Predictor features consisted of multi-temporal change metrics and single-date reflectance values derived from the VGT composites for the period April 21-October 10, 1998. The change metrics were defined by 10- and 30-day changes in reflectance (red, NIR, and SWIR channels) and in two vegetation indices (VI): NDVI and an analogous SWIR based VI (SWVI) that is sensitive to boreal burns (Fraser et al., 2000b). The 10-day changes were computed by differencing pixel reflectance or VI values from two consecutive 10-day periods. 30-day metrics were based on the cumulative 30-day change surrounding each corresponding 10-day change. For example, NIR change metrics to predict the probability of pixel being burned at time (t) were computed as:

$$\Delta NIR_{10} = NIR_t - NIR_{t-1} \qquad\qquad\qquad [1]$$

$$\Delta NIR_{30} = NIR_{t+1} - NIR_{t-2} \qquad\qquad\qquad [2]$$

where: ΔNIR_{10} = pixel's 10-day change in NIR reflectance

ΔNIR_{30} = pixel's 30-day change in NIR reflectance surrounding the 10-day change

t = the 10-day period during which burning potentially occurred
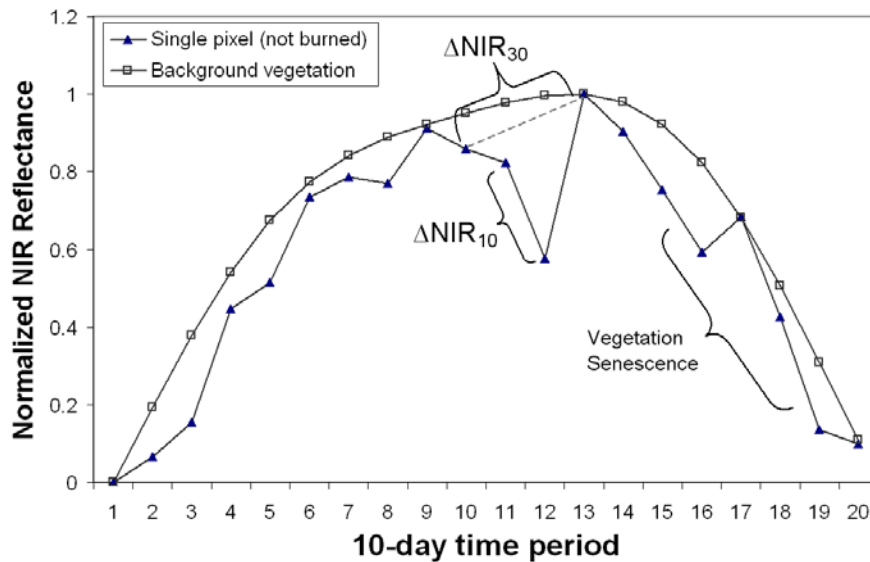
Figure 1. The curves show 10-day and 30-day changes in NIR reflectance changes for an unburned pixel (triangle symbols) and its background vegetation (square symbols) based on a hypothetical time series of 10-day composites over a growing season. The 30-day changes can be useful to identify spurious 10-day drops in reflectance, while normalization to the background trajectory will control for reflectance decreases during the fall senescence period (right portion of curve).

The triangle symbols in figure 1 illustrate 10- and 30-day NIR changes for a single pixel based on a hypothetical time series of 10-day composites over a growing season. In this case the pixel has not burned, yet is subject to a large single-date drop in reflectance that could cause a change detection algorithm to misclassify it as burned. Such ephemeral decreases are commonly observed in coarse resolution imagery and may be caused by a number of factors such as cloud shadow, shifts in viewing geometry, sub-pixel cloud contamination in the previous composite, or small shifts in image registration against an adjacent dark object like water. The addition of a surrounding 30-day change metric may aid in identifying such a false burn signal flagged by a 10-day change, as the pixel will be less likely to also have a large corresponding 30-day reflectance drop. By contrast, the reflectance of burned forest in the boreal zone recovers over a period of several weeks to months (Fraser et al., 2000) and should be flagged by both a 10-day and surrounding 30-day metric.
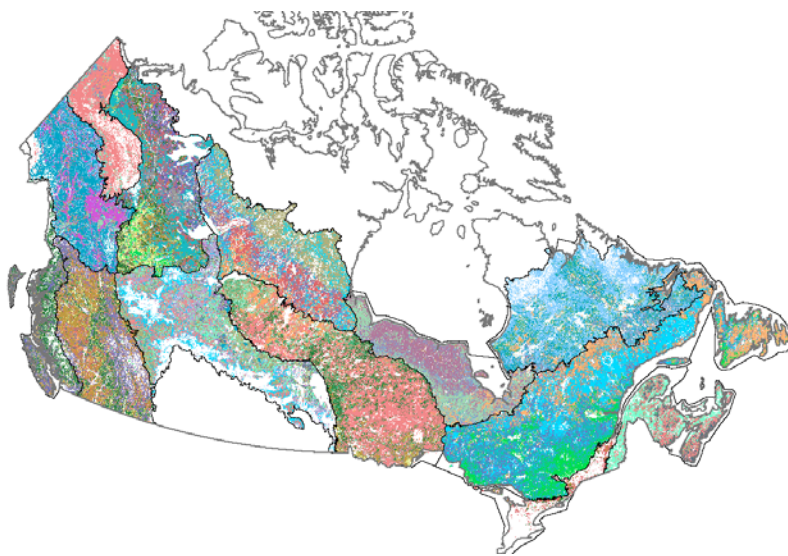
Figure 2. Canada-wide distribution of forested pixels to which the burned area mapping algorithm was applied. The various colours represent 117 background vegetation clusters that were produced by grouping nine forest-related cover types within 13 Canadian terrestrial ecozones. The vegetation clusters are used to normalize each pixel's 10- and 30-day change metric to account for phenological variation.

Two special features of the change metrics were considered for their calculation. First, each pixel's 10- and 30-day change was normalized to the reflectance trajectory of similar background vegetation, which is illustrated by the square symbols in figure 1. This normalization, referred to as modified delta space thresholding by Zhan et al. (2000), accounts for reflectance changes attributable to seasonal vegetation phenology. In the case of boreal forest, decreasing NIR reflectance of understory vegetation during the fall senescence period (right portion of curve) will make multi-temporal algorithms especially susceptible to producing false alarms. In this application, the background vegetation groupings were based on nine forest-related cover types

derived from a VGT classification (Latifovic et al., 2002) stratified over 13 Canadian terrestrial ecozones, which are defined by having similar climate, geology, and flora (figure 2; Ecological Stratification Working Group, 1996). The ecozone stratification was included mainly to adjust for north-south differences in the timing of the growing season. This cover type-ecozone intersection produced a total of 117 background vegetation groupings across Canada (figure 2). The normalization may be expressed for the NIR channel as:

$$\delta NIR_{10} = \Delta NIR_{10} - \Delta NIR_{10b} \qquad\qquad [3]$$

where: δNIR_{10} = normalized 10-day change in reflectance

ΔNIR_{10b} = 10-day NIR reflectance change in background vegetation

A second feature applied to the change metrics is that any pixels in the nominally clear 10-day composites contaminated by snow or atmosphere (e.g. cloud, smoke) were skipped. In our algorithm development and application using 1998-2000 VGT data, pixels were flagged as contaminated if red reflectance was greater than three standard deviations from the mean growing season (July-August) reflectance of their respective vegetation groupings defined above. A maximum 7% red reflectance was enforced for all pixels to control for the high variation observed in mountainous areas of Canada. Note that these thresholds were designed to be conservative (mean 6%, range 1.5-7%) to limit the large fluctuation in reflectance and potential false burn signal that may occur from sub-pixel cloud contamination or in mountainous areas.

In addition to the metrics describing relative changes between composites, we examined independent variables representing absolute reflectance and VI values. These were extracted for each current and previous 10-day period (e.g. NIR_t and NIR_{t-1}). A total of 20 independent variables was thus computed from three reflectance channels and two VIs for each pixel.

To develop a regression model from the training sample, the change metrics and reflectance features were identified for each pixel corresponding to the 1998 composite period that demonstrated the largest normalized drop in NIR reflectance (Equation 2). Given the significant immediate decrease in NIR reflectance observed in burned boreal forest (Fraser et al., 2000b), it was assumed that this criterion would effectively select the actual date of burning for the burned training pixels. Furthermore, in the unburned training sites it would select the

composite date that most closely resembles a true burn signal, thereby presenting the most challenging case for the logistic model.

Before combining the features into a multiple logistic regression model, each candidate change metric was evaluated independently by deriving a single variable logistic model. The regression models were compared using McFadden's Rho-squared statistic (Steinberg and Colla, 2000), a transformation of the likelihood-ratio statistic. Rho-squared ranges between 0 and 1 and mimics the R^2 coefficient of determination, although it tends to produce smaller values. A measure of overall prediction success also was computed that summarized the

Figure 3. Histograms showing the distribution of maximum 30-day changes of burned and unburned training samples for the single best change metric (SWVI vegetation index).

classificatory power of the regressions. Prediction success was represented by the output logistic regression probabilities (ranging from 0-1) averaged over all training samples. Table 1 summarizes the results from the single feature comparison based on the logistic model Rho-squared and prediction success. The change in NIR reflectance (δNIR_{10}, δNIR_{30}) provided the best VGT channel separation of burned areas, measured both at 10- and 30-day intervals. The NIR region typically demonstrates the strongest response after burning due to the destruction of highly scattering, leafy vegetation (Pereira et al., 1999). The best single feature for discriminating burned forest based on both Rho-squared (0.59) and prediction success (0.84) was the 30-day change in the SWVI, which combines the NIR and SWIR channels. Figure 3 shows the distribution of maximum 30-day SWVI changes for the burned and unburned training samples. The superiority of the NIR-SWIR spectral space for burned area detection agrees with recent studies examining a range of vegetation types (Pereira, 1999, Fraser et al., 2000b).

A multiple logistic regression model to combine the 20 candidate features was developed based on a backward stepwise procedure. Beginning with all variables, the feature with highest probability value was manually removed at each step until only one remained. The criteria used

to select the "best" overall model from the set of models containing between 1-20 variables were the explanatory power of the models measured from Rho-squared, balanced by the computational demand required by a model having additional parameters. Based on this trade-off, the stepwise model containing four features—two 10-day and two 30-day metrics—was chosen (Rho-squared=0.77; p< 0.005; equation 5). By comparison, a multiple regression model with three variables produced a 0.03 decrease in Rho-squared, while models containing more than four variables provided only modest improvements. For example, the ten parameter model increased Rho-squared by only 0.03 to 0.80.

$$p(burned) = \frac{1}{1+e^{-\left(4.7+0.216\times\delta SWVI_{10}+0.033\times\delta SWIR_{10}+0.217\times\delta NDVI_{30}+0.072\times\delta \operatorname{Re} d_{30}\right)}} \quad [4]$$

Where:

p(burned) = probability of a pixel being burned during a 10-day interval

δSWVI10 = normalized 10-day change in a short-wave based vegetation index (SWVI)

computed as $\frac{NIR-SWIR}{NIR+SWIR}\times100$

δSWIR10 = normalized 10-day change in SWIR reflectance (scaled from 0-2000)

δNDVI30 = normalized 30-day change in NDVI surrounding the current 10-day interval (i.e.

δNDVI10$_{t-1}$ + δNDVI10$_{t}$ + δNDVI10$_{t+1}$)

δRed30 = normalized 30-day change in Red reflectance (scaled from 0-2000)

Selecting an optimal probability threshold

Equation [4] was applied across Canada to the time series of VGT composites from the 1998 training year. The maximum per-pixel probability obtained from the model among all 10-day periods is presented as an annual probability-of-burning map shown in figure 4. A separate output channel was used to record the 10-day time period during which the highest probability

occurred. This probabilistic or "soft" output provided by logistic regression is more flexible

compared to traditional "hard" change detection approaches in that it provides a confidence level

for the change product (Morisette et al., 1999). A suitable probability level can then be tailored

to specific applications where the consequences of omission and commission error vary

(Morisette and Khorram, 2000). For example, if the burned area model were designed as a first-

pass filter to target all areas potentially subject to burning for further examination, a smaller,

more liberal threshold could be selected.
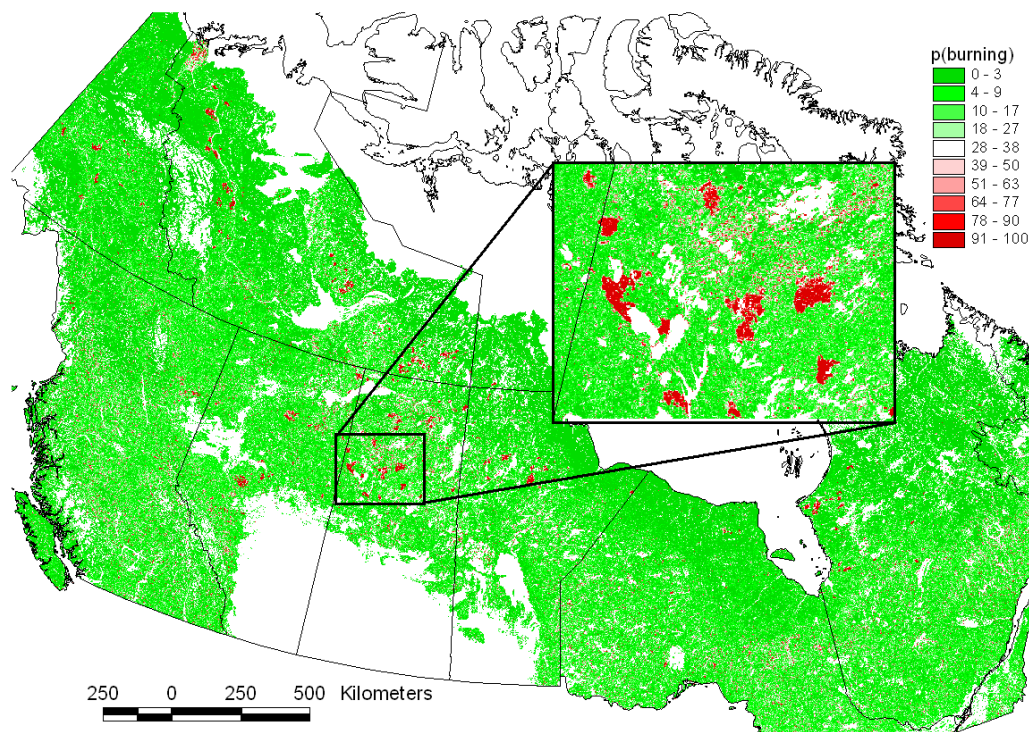
Figure 4. Maximum probability (scaled from 0-100) of burning from the multiple logistic
regression model applied to all 10-day periods in 1998.

To derive a binary burned area mask from the maximum logistic regression output, a cut-

off probability threshold must be specified. In logistic modelling applications, a 0.5 threshold is

often adopted under the assumption that it will provide a balance between omission (missed

burns) and commission (false burns) error. For this application, the decision threshold was

optimized by applying the model to the 1998 training samples and then quantifying error rates

over a range of output probabilities. Figure 5a shows plots of commission, omission, and overall

error in the training data for probabilities ranging from 0.05-0.97. A probability of 0.4 was

found to balance the two types of error and provide the smallest overall error of 6.4%. The resulting burned area mask (sample area shown in figure 5a) captured the burned areas effectively by comparison to 1998 fire surveys, but obviously produced an unacceptable number of falsely classified burned pixels. The Canada-wide mask contained a burned area of 35.5 million ha in year when there were only 4.7 million ha reported burned by Canadian fire management agencies.

The result obtained from the initial 0.4 threshold underscores a general challenge for continental scale, satellite-based burned area mapping. Since in many ecosystems burning affects a disproportionately small area of vegetation in a single year (e.g. about 0.5% of Canadian forest), a given susceptibility to commission error will produce a much larger area of misclassified pixels than the same rate of omission error. For example, to achieve less than 20% commission error over Canada in an average year, a 10-day burned area algorithm must incorrectly label fewer than about 1 in 14,000 pixels at each time step (i.e. 380,422,000 ha of forest $\times$ 0.00007356 error rate $\times$ 24 composite dates = 671,600 ha). This bias is not accounted for by balancing the commission and omission errors in the training data that have a similar number of burned and unburned samples.

One means of controlling for the bias is to derive an area-adjusted error that estimates the likely *area* of commission and omission errors produced at a continental scale over a range of thresholds. Area-based errors were approximated by multiplying at each probability level, the percent omission error by a typical annual burned area for Canada (we use the 10-year average of 3,358,000 ha) and multiplying the percent commission error by the area of forested pixels over which the algorithm is applied (380,422,000 ha). Based on these area-adjusted errors (figure 5b), a threshold of 0.97 was predicted to balance the total area of missed burned pixels and false burned pixels mapped at a national scale. The resulting burned area mask from this second, conservative threshold was found to have much smaller levels of noise than that produced by the 0.4 threshold, but at the expense of missing a portion of the true burned areas (figure 5b right).
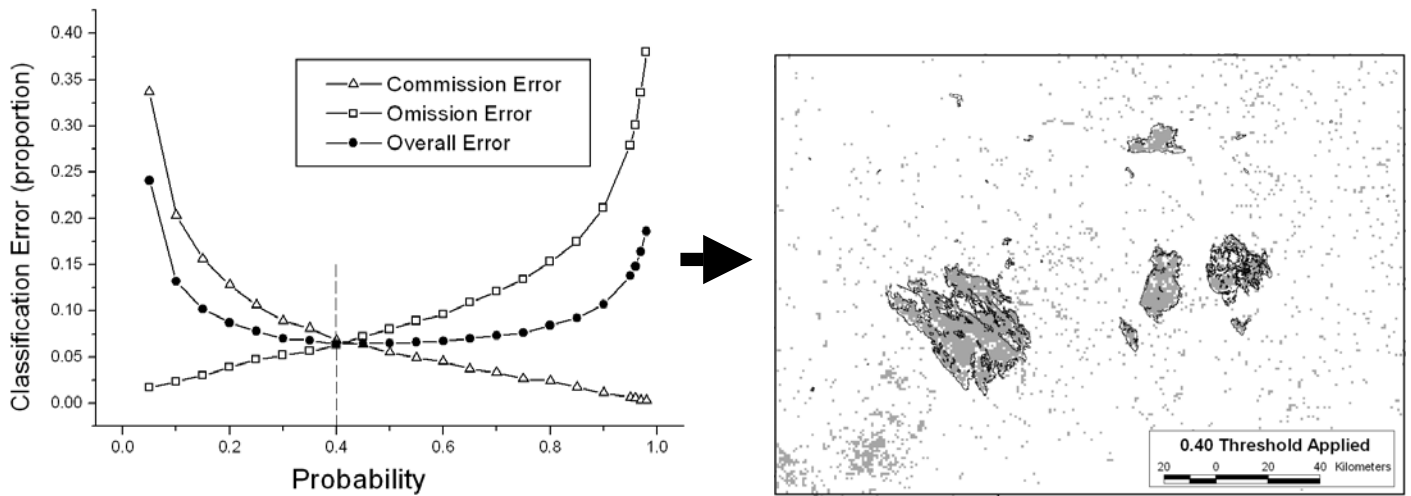
Figure 5a. Accuracy assessment curves showing rates of commission error, omission error, and overall error in the training data set over a range of output probabilities from the logistic model. The image on the right shows a typical burned area mask (grey pixels) based on the probability level (0.4) that produces the lowest overall rate of error.
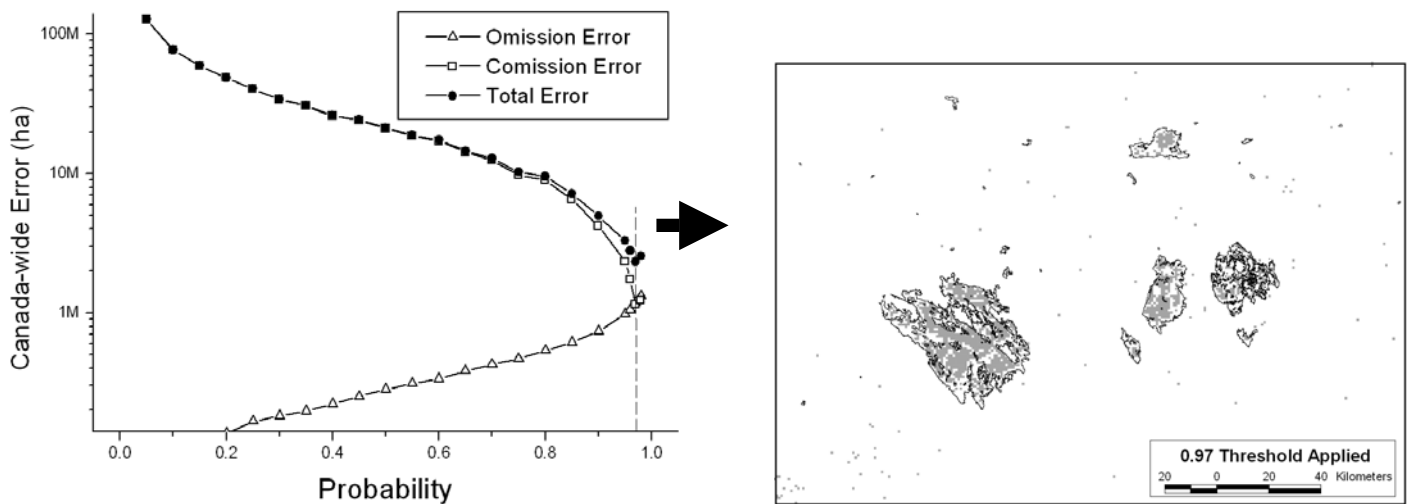
Figure 5b. Accuracy curves showing the predicted national-level *area* of the various errors in the training data set over a range of probabilities. The image shows resulting burned area (grey pixels) based on the probability level (0.97) that is predicted to produce the smallest area of misclassified pixels. Provincial forest fire surveys are outlined in black

Post-regression contextual tests

The 0.97 probability threshold derived above should produce a burn mask with the lowest overall Canada-wide error from the per-pixel logistic regression model and satellite change metrics. When examining this mask against 1998 fire surveys covering the provinces of Alberta and Saskatchewan, we noted two limitations. First, although most burns were reliably identified, the conservative 0.97 threshold caused underestimation of their areas (e.g., figure 5b right). According the error curves in figure 5a, this threshold led to 34% of the burned pixels in the training set being mapped as unburned. A second deficiency was the presence of salt-and-pepper noise from burned clusters composed of just one or a few pixels. Although these were small relative to the correctly mapped burned areas, they were far more numerous and their combined area at a national scale was significant. For example, pixel clusters smaller than 5 pixels (500 ha) accounted for 1,208,500 ha or 39% of the burned area in this 1998 logistic product. By contrast, 1998 fire statistics for Canada indicate that fires smaller than 1,000 ha (10 pixels) accounted for only 2.4 percent of the burned area (Canadian Forest Service National Forestry Database Program; http://nfdp.ccfm.org/).

To remedy these limitations in the pixel-based regression model that exploits reflectance information only, a series of spatial-contextual tests was developed. These were designed to decrease noise and increase the sensitivity of detection by means of a spatial contraction then expansion of the logistic burned area mask. Figure 6 illustrates the general steps required by the burn mapping procedure, including contextual tests (steps 5-6).

1. The first test requires eliminating any contiguous burned area cluster composed of fewer than six pixels (figure 6, step 5). Considering that, over the 10-year period between 1989-1998, fires smaller than 1,000 ha (10 pixels) accounted for only 3% of the national burned area, this filter eliminated most of the of commission error, while removing only a fraction of the correctly mapped burned area.

2. The second test uses the remaining filtered high-probability pixels as "seeds" from which the burns were iteratively grown to lower probability pixels (figure 6, step 6). Based on the 1998 Alberta and Saskatchewan fire survey data, the best result was obtained when region growing is permitted to adjacent pixels with a burned area probability ≥ 0.35. Note that any burned pixels adjacent to water bodies were filtered before this step to account for false burns that may arise due to sub-pixel, multi-temporal misregistration.
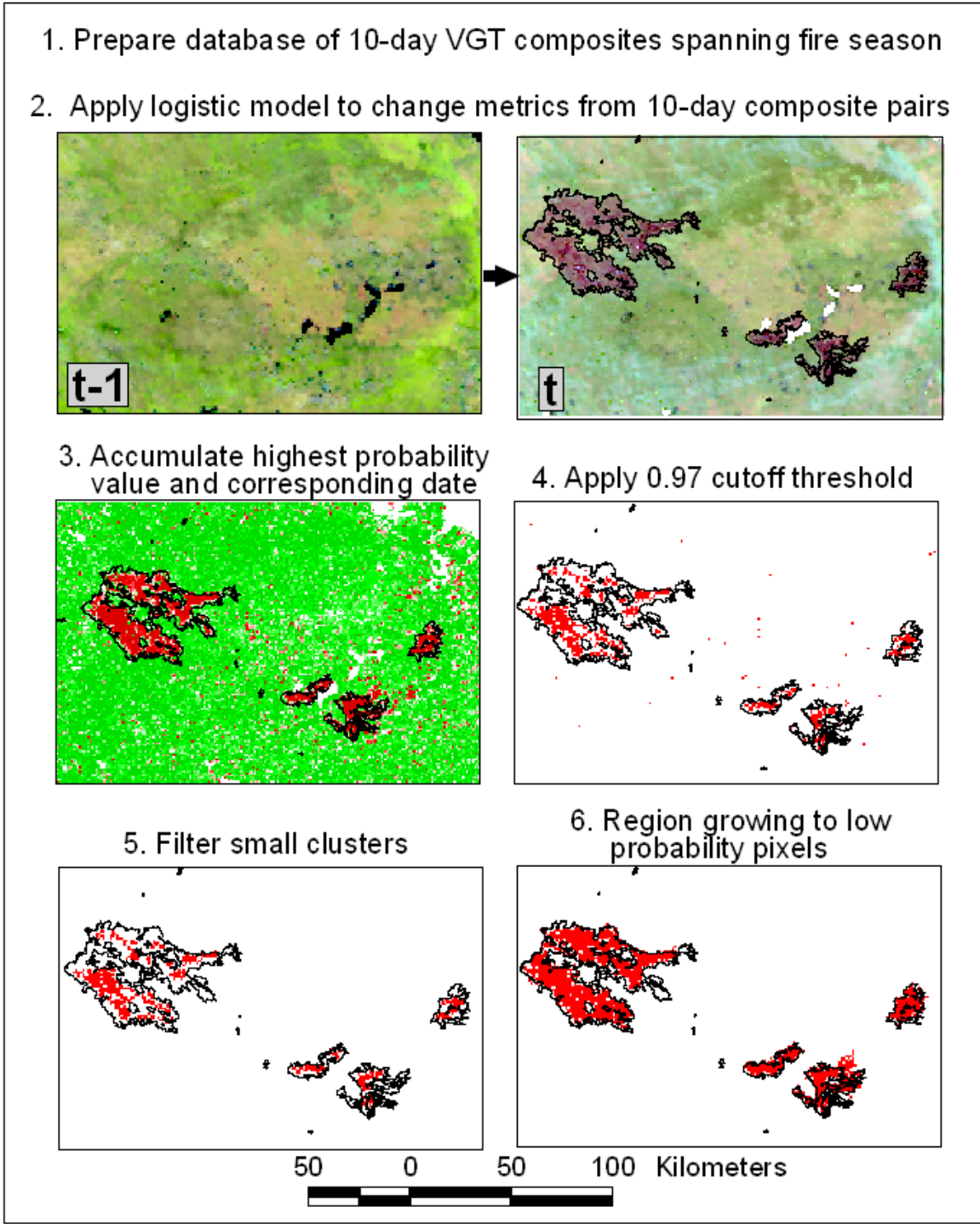
Figure 6. Steps required for 10-day burned area mapping using the procedure described in this paper. Step 2 shows pre- and post-burn false colour VGT composites (R,G,B=SWIR, NIR, Red). Probability levels in step 3 are displayed using the same colour palette shown in figure 4. In steps 4-6, algorithm results are shown in red with the provincial burned area survey outlined in black. Steps 2-6 are automated using an ARC/INFO GIS macro.

3. The third contextual test requires that each of the grown burn patches be composed of at least 15% high probability pixels (not shown in figure 6). This test was effective in removing false burns in a few cases where a small cluster of non-burned pixels with high probability grew over a large area of medium probability pixels. This test removed very few real burns, as these typically contained a much larger proportion of high probability pixels.

ALGORITHM VALIDATION

The procedure described above was applied to produce Canada-wide burned area masks for the 1998-2000 forest fire seasons using a GIS script that (1) calculates a logistic probability for each 10-day time period; (2) selects the highest annual probability for each pixel; and (3) applies the spatial/contextual tests (figure 6). Resulting burned area masks for the three years are presented in Figure 7, where 1998 burns area shown in red, 1999 in green, and 2000 in blue. The VGT product consistently contained smaller national level burned areas by comparison to official statistics compiled by CIFFC. The estimated burned area for 1998-2000 was 3,900,100 ha, 1,425,800 ha, and 631,100 ha, which is respectively 17.2%, 16.4%, and 2.5% smaller than CIFFC estimates of 4,710,775 ha, 1,705,645 ha, and 647,071 ha.

A regional-level comparison of burned area by province/territory is presented in Figure 8. The three provinces not shown (NS, NB, and PEI) all had CIFFC burned areas smaller than 2000 ha and no VGT-mapped burns. Over the three years, most of the province-level VGT burned areas compared reasonably well to the official estimates from fire management agencies, with burned area being typically underestimated to the same extent as in the national-level statistics. The weakest performance of the satellite algorithm was observed for a few provinces in 2000, when a relatively small area burned in Canada. In Quebec, Yukon, and B.C., burned area overestimation was due to a small number of large, false burn patches that appeared to be caused by cloud shadow and topographic effects. In Canada, periods with high fire activity in Canada are typically preceded by long sequences of clear, dry days (Flannigan and Wotton, 2001). In 2000, burned area was significantly below average and the 10-day VGT images had relatively high levels of cloud contamination and cloud shadowing, which can respectively produce burn omissions and commissions.
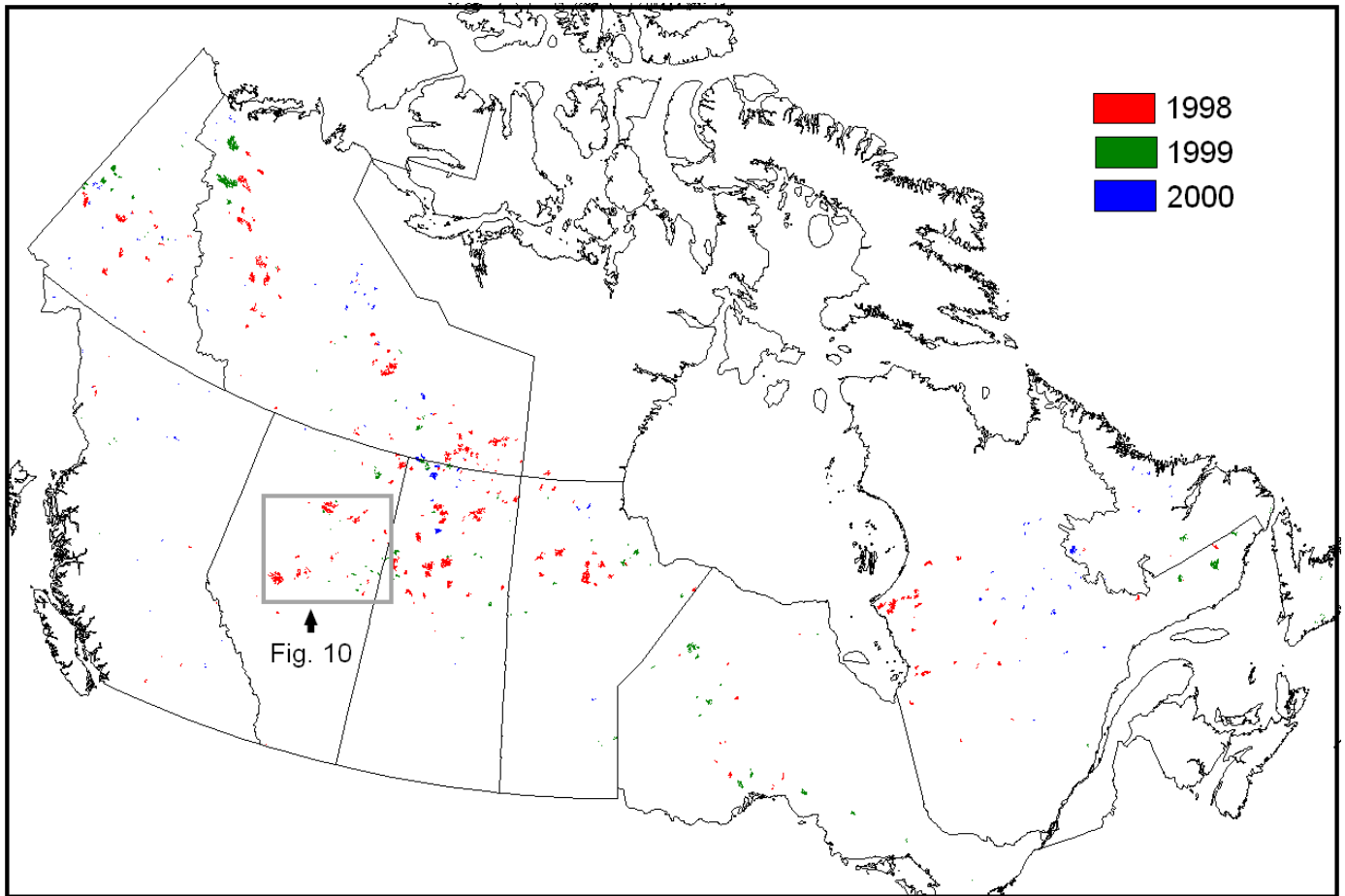
Figure 7. National-level burned area masks for 1998 (red), 1999 (green), and 2000 (blue) produced using the satellite-based 10-day burned area algorithm.

Falsely mapped burns were identified at a national scale for the three years by verifying the 431 VGT-mapped burns in figure 7 with changes visible in September VGT composite images before and after each fire season, and the presence of active fires identified using daily NOAA-AVHRR imagery. There was no evidence of fire activity for 60 of the satellite-mapped burns, which represented commission errors of 0.28% for 1998 (4 clusters covering 10,800 ha), 5.5% for 1999 (22 clusters and 78,100 ha), and 19.2% for 2000 (34 clusters and 121,300 ha). Total commission error was largest in 2000, with percent commission error being magnified further due to the small level of burning (note the smaller x-axis scale in figure 8c).

A more detailed assessment of the satellite burned area mask was performed using burned area surveys produced by fire management agencies in Alberta and Saskatchewan from

Figure 8.

(a)
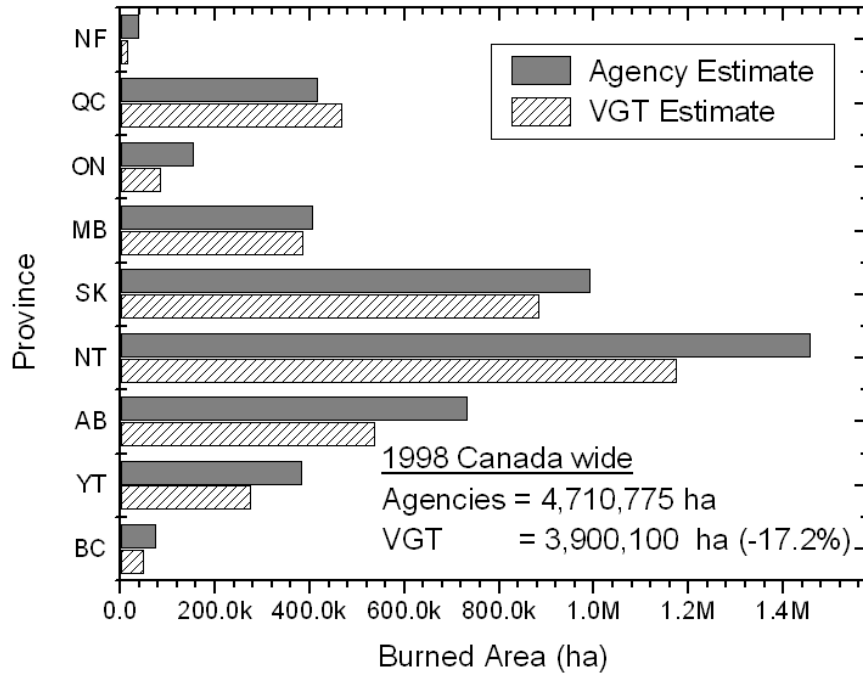
(b)
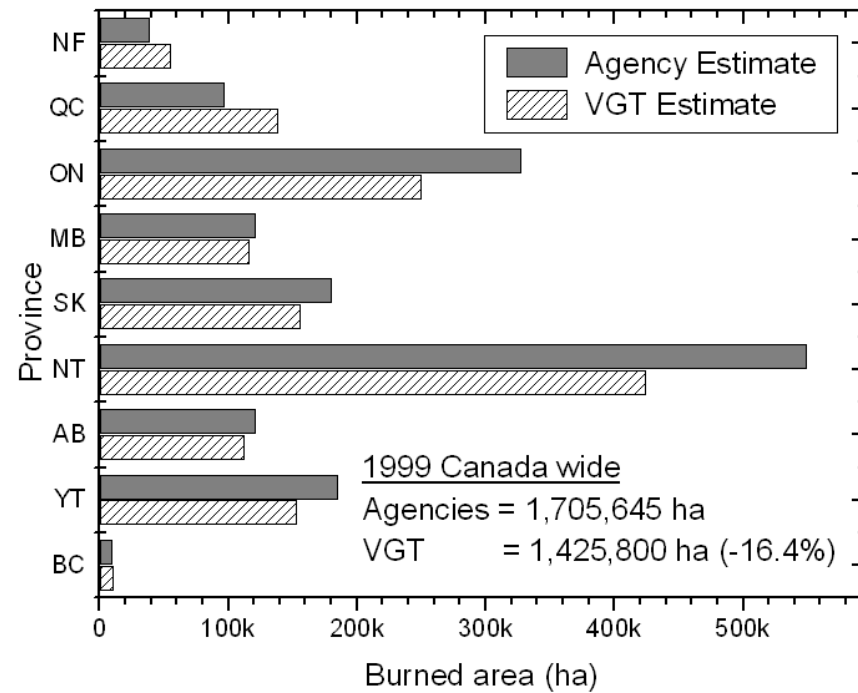
(c)
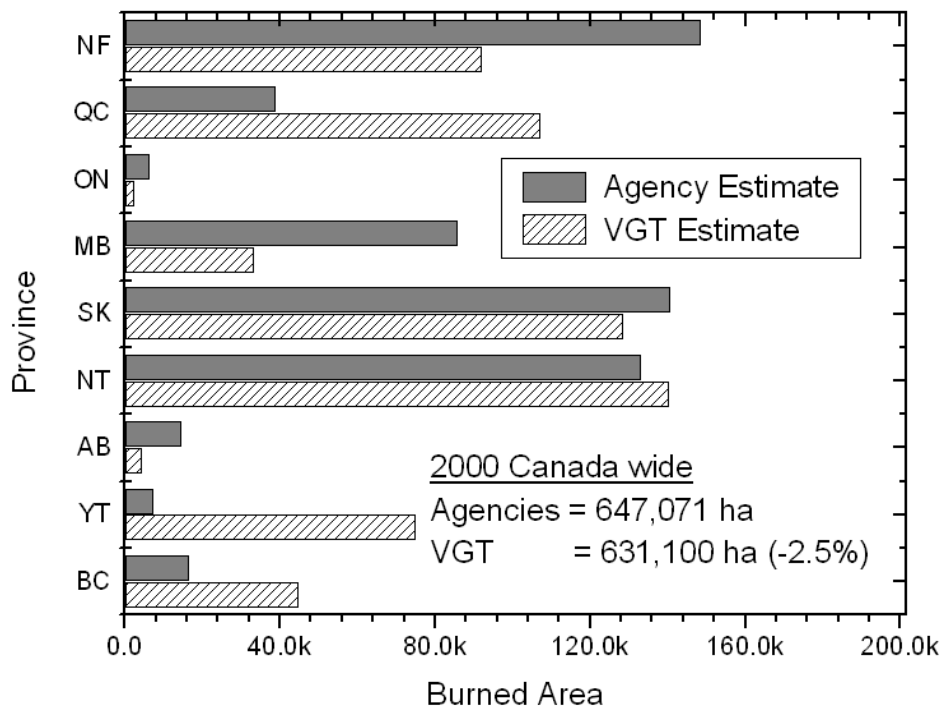
Figure 8. Bar graphs comparing burned area by province based on official fire management agency statistics and the VGT-based mapping algorithm for (a) 1998, (b), 1999, and (c) 2000.

GPS and photo-interpretation. The available 1998-2000 Alberta and 1998-1999 Saskatchewan burned area surveys cover 1.74 million ha, or 25% of the 1998-2000 national burned area. By comparison, the VGT product mapped 1.65 million ha burned in these provinces during the same periods, of which 31,300 ha was not associated with real fires, representing a commission error of 2%. In terms of omission error, VGT did not map 496 of the 587 fires in the two provinces; however, these fires were mostly small and together comprise only 198,912, or 11.4%, of the 1.74 million ha of burned forest.

The relationship between the corresponding areas of individual burns from the fire agency surveys and satellite algorithm is shown in figure 9. The overall relationship was strong (full sample, $R^2 = 0.84$, p < 0.005, n=587; VGT-mapped burns, $R^2 = 0.90$, P<0.005, n = 91) with better mapping accuracy for fires larger than about 1,000 ha, which is similar to results from previous boreal burn mapping applications using NOAA/AVHRR
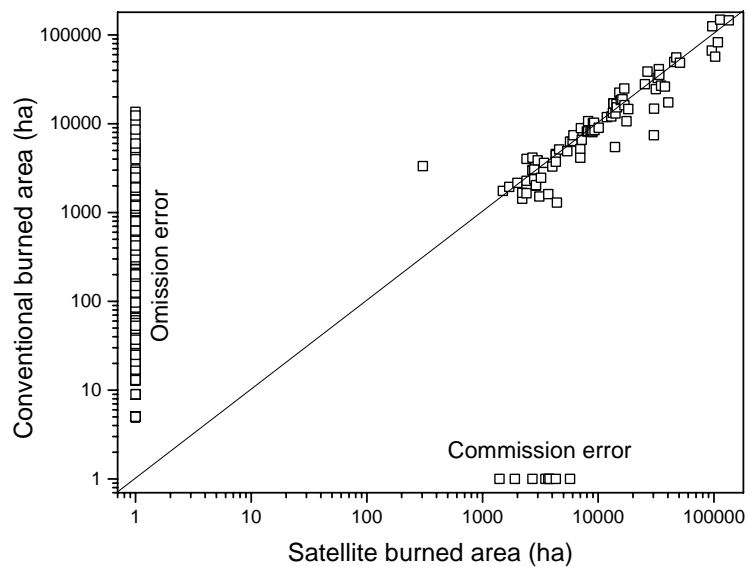
Figure 9. The relationship between the individual burned areas mapped by the fire agencies in Alberta (1998-2000) and Saskatchewan (1998-1999) and the satellite mapping algorithm. The line indicates a 1:1 relationship, and a log-log scale is used to improve visualization of the distribution.

(Kasischke and French, 1995; Fraser et al., 2000). Figure 10 illustrates the above statistical results by comparing the VGT mask and fire surveys for a region in Alberta subjected to a range of fires sizes. Note that some of the missed areas within larger burns were likely attributable to VGT not being able to detect surface burning where they was little or no damage to the tree crowns above.

The technique presented here provides generally similar performance to the HANDS algorithm developed for annual mapping of burned boreal forest (Fraser et al., 2000a). Both
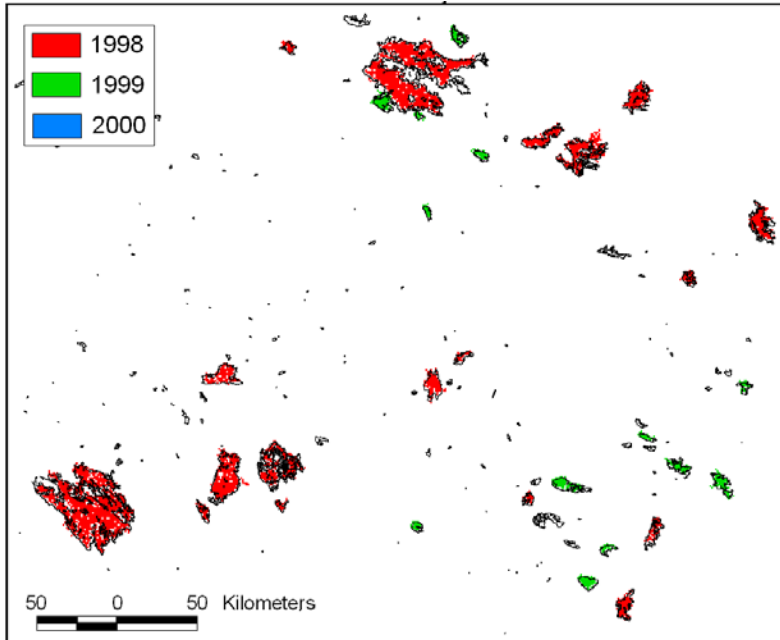
Figure 10. VGT burned area mask (1998 = red, 1999=blue, 2000=green) for a region in Alberta (location shown in figure 7) subject to a range of fire sizes. Burn surveys produced by the provincial fire management agencies are shown outlined in black.

techniques (a) consistently produce national-level burned areas within ~ 15% of Canadian fire agency statistics; (b) are best suited for mapping burns larger than 10 km^2; and (c) produce commission errors, in terms of the area of falsely mapped burns, on the order of 5%. The HANDS technique relies only on anniversary-date clear-sky composites for the end of each fire season, yet also requires an annual active fire detection (hotspot) mask that reliably identifies all the burns to be mapped. However, the availability of multiple satellite sensors and systems providing fire detection products (e.g. AVHRR, MODIS, ATSR, GOES) now makes compiling such masks more feasible. HANDS has produced more reliable results for years when there is significant cloud cover (and image contamination) and relatively little fire activity (e.g. 2000), while its use of active fire locations for local training makes it more adaptable to different vegetation types (Li et al., 2002). The logistic regression-based technique requires only a series of corrected, cloud-screened VGT composites covering the fire season. The main advantages of this technique are that it provides 10-day temporal resolution and does not need the input of an active fire detection mask.

SUMMARY AND CONCLUSIONS

This paper presented a technique for mapping burned areas in the boreal forest zone at 10-day intervals using coarse resolution satellite imagery. The major findings and conclusions from the work are as follows.

1. Logistic regression is a flexible statistical approach for burned area mapping, since it can be used to compare satellite-based change metrics and select the most effective combination of metrics. It also produces an output that represents probability of burning, to which an optimal cut-off probability level can be applied to achieve the desired balance between omission and commission error.

2. 10-day burned area mapping using VGT and the procedure described in this paper can produce burned area masks that accurately detect most burns > 10 km^2, while producing relatively few false fires (3.5% of 1998-2000 burned area). A large number of small burns (< 10 km^2) that were not mapped contribute little to the total burned area in boreal environments.

3. The performance of the burn mapping algorithm was reduced when applied to the 2000 fire season in Canada, a year with relatively little fire activity. This was attributable to increased cloud cover and cloud shadow, a smaller frequency of very large burns, and a greater ratio between the area of commission error and actual area burned.

REFERENCES

Cahoon, D.R., Stocks, B.J., Levine, J.S., Cofer, W.R., and Pierson, J.M. 1994. Satellite analysis of the severe 1987 forest fires in northern China and southeastern Siberia. *Journal of Geophysical Research,* 99:18,627-18,638.

Crutzen, P.J., and Andreae, M.O. 1990. Biomass burning in the tropics: impact on atmospheric chemistry and biogeochemical cycles. *Science,* 250:1669-1678.

Ecological Stratification Working Group. 1996. *A National Ecological Framework for Canada.* Agriculture and Agri-Food Canada, Research Branch, Centre for Land and Biological Resources Research and Environment Canada, State of Environment Directorate.

FAO (Food and Agriculture Organisation). 2001. Global Forest Fire Assessment 1990-2000. FRA Working Paper No. 55. www.fao.org/forestry/fo/fra/index.jsp.

Flannigan, M.D., and Wotton, B.M. 2001. Climate, weather, and area burned. In *Forest Fires.* pp. 351-373. Academic Press.

Fraser, R.H., Li, Z., and Cihlar, J. 2000a. Hotspot and NDVI Differencing Synergy (HANDS): a new technique for burned area mapping over boreal forest. *Remote Sensing of Environment*, 74:362-376.

Fraser, R.H., Li, Z., and Landry, R. 2000b. SPOT VEGETATION for characterising boreal forest fires. *International Journal of Remote Sensing,* 21: 3525-3532.

Kasischke, E.S., and French, N.H. 1995. Locating and estimating the areal extent of wildfires in Alaskan boreal forests using multiple-season AVHRR NDVI composite data. *Remote Sensing of Environment,* 51:263-275.

Koutsias, N., and Karteris, M. 1998. Logistic regression modelling of multitemporal Thematic Mapper data for burned area mapping. *International Journal of Remote Sensing,* 19(18):3499-3514.

Koutsias, N., and Karteris, M. 2000. Burned area mapping using logistic regression modeling of a single post-fire Landsat-5 Thematic Mapper image. *International Journal of Remote Sensing,* 21(4):673-687.

Latifovic, R., Cihlar, J., and Chen, J., 2002. A comparison of BRDF models for the normalisation of satellite optical data to a standard viewing geometry. Accepted for *IEEE Transactions on Geoscience and Remote Sensing.*

Li, Z., Nadon, S. and Cihlar, J. 2000. Satellite detection of Canadian boreal forest fires: Development and application of an algorithm. *International Journal of Remote Sensing,* 21: 3057-3069.

Li, Z., Fraser, R., Jin, J., Abuelgasim, A.A., Csiszar, I., Gong, P., Pu, R., and Hao, W. 2002. Evaluation of algorithms for fire detection and mapping across North America from satellite. Under revision for *Journal of Geophysical Research*.

Luther, J.E., Franklin, S.E., Hudak, J., and Meades, J.P. 1997. Forecasting the susceptibility and vulnerability of balsam fir stands to insect defoliation with Landsat Thematic Mapper data. *Remote Sensing of Environment,* 59:77-91.

Martell, D.L., Otukol, S., and Stocks, B.J. 1987. A logistic model for predicting daily people-caused fire occurrence in Ontario. *Canadian Journal of Forest Research,* 17:394-401.

Michener, W.K., and Houhoulis, P.F. 1997. Detection of vegetation changes associated with extensive flooding in a forested ecosystem. *Photogrammetric Engineering & Remote Sensing,* 63(12):1363-1374.

Morisette, J.T., Khorram, S., and Mace, T. 1999. Land-cover change detection enhanced with generalized linear models. *International Journal of Remote Sensing, 20(14):* 2703-2721.

Morisette, J.T., and Khorram, S. 2000. Accuracy assessment curves for satellite-based change detection. *Photogrammetric Engineering & Remote Sensing,* 66(7):875-880.

Narumalani, S., Jensen, J.R., Althausen, J.D., Burkhalter, S., and Mackey, H.E. 1997. Aquatic macrophyte modeling using GIS and logistic multiple regression. *Photogrammetric Engineering & Remote Sensing,* 63(1):41-49.

Pereira, J.M.C., and Itami, R.M. 1991. GIS-based habitat modeling using logistic multiple regression: a study of the Mt. Graham red squirrel. *Photogrammetric Engineering & Remote Sensing,* 57(11):1475-1486.

Pereira, J.M.C. 1999. A comparative evaluation of NOAA/AVHRR vegetation indexes for burned surface detection and mapping. *IEEE Transactions on Geoscience and Remote Sensing* 37(1):217-226.

Pereira, J.M.C., Sa, A.C.L., Sousa, A.M.O., Silva, J.M.N., Santos, T.N., and Carreiras, J.M.B. 1999. Spectral characterisation and discrimination of burnt areas. In *Remote Sensing of Large Wildfires*, edited by E. Chuvieco (Berlin: Springer-Verlage), pp. 123-138.

Rahman, H., and Dedieu, G. 1994. SMAC: a simplified method for atmospheric correction of satellite measurements in the solar spectrum. *International Journal of Remote Sensing,* 15:123-143.

Siegert, F., and Hoffmann, A.A. 2000. The 1998 forest fires in East Kalimantan (Indonesia): a quantitative evaluation using high resolution, multitemporal ERS-2 SAR images and NOAA-AVHRR hotspot data. *Remote Sensing of Environment,* 72:64-77.

Steinberg, D. and Colla, P. 2000. Logistic Regression. In: *SYSTAT 10 Statistics I.* pp. 549-616. SPSS, Chicago, IL.

Stocks, B.J. 2001. Fire Management in Canada. In: *Global Forest Fire Assessment 1990-2000.* FRA Working Paper No. 55. pp. 404-408. www.fao.org/forestry/fo/fra/index.jsp

Vega Garcia, C., Woodard, P.M., Titus, S.J., Adamowicz, W.L., and Lee, B.S. 1995. A logit model for predicting the daily occurrence of human caused forest fires. *International Journal of Wildland Fire,* 5(2):101-111.

Zhan, X., Defries, R., Townshend, J.R.G., Dimiceli, C., Hansen, M., Huang, C., and Sohlberg, R. 2000. The 250 m global land cover change product from the Moderate Resolution Imaging Spectroradiometer of NASA's Earth Observing System. *International Journal of Remote Sensing,* 21(6-7):1433-1460.

Table 1. Assessment of individual change metrics based on the Rho-squared statistic and overall prediction success. The variables denoted by δx_{10} refer to a 10-day normalized change measured on the date corresponding to the largest drop in NIR reflectance. The surrounding 30-day normalized change is δx_{30}, x_t is the value measured on the date of maximum NIR drop, and x_{t-1} is the value measured in the previous composite. The best four predictors according to each statistic are shown in bold.

Independent variable	Rho-squared statistic	Overall prediction success
δRed_{10}	0.01	0.51
δNIR_{10}	**0.51**	**0.80**
$\delta SWIR_{10}$	0.01	0.51
$\delta NDVI_{10}$	0.38	0.73
$\delta SWVI_{10}$	**0.53**	**0.80**
δRed_{30}	0.05	0.54
δNIR_{30}	**0.53**	**0.82**
$\delta SWIR_{30}$	<0.00	0.50
$\delta NDVI_{30}$	0.46	0.77
$\delta SWVI_{30}$	**0.59**	**0.84**
Red_t	0.01	0.53
NIR_t	0.44	0.76
$SWIR_t$	0.05	0.53
$NDVI_t$	0.29	0.68
$SWVI_t$	0.29	0.68
Red_{t-1}	0.01	0.50
NIR_{t-1}	0.03	0.52
$SWIR_{t-1}$	0.02	0.50
$NDVI_{t-1}$	NS	NS
$SWVI_{t-1}$	NS	NS